Vectorial insertion of a β-helical peptide into membrane: a theoretical study on polytheonamide B

Vectorial insertion of a β-helical peptide into membrane: A theoretical study on polytheonamide B

Mahroof Kalathingal,[1] Takashi Sumikama,[2,3] Shigetoshi Oiki,[*4] and Shinji Saito[*1,5]

[1]School of Physical Sciences, The Graduate University for Advanced Studies, Okazaki, Aichi 444-8585, Japan

[2]PRESTO, JST, Kawaguchi, Saitama 332-0012, Japan

[3]Nano Life Science Institute (WPI-NanoLSI), Kanazawa University, Kanazawa 920-1192, Japan

[4] Biomedical Imaging Research Center, University of Fukui, Fukui 910-1193, Japan

[5]Institute for Molecular Science, Okazaki, Aichi 444-8585, Japan

Condensed running title: Vectorial insertion of pTB

ABSTRACT

Spontaneous unidirectional, i.e., vectorial, insertion of transmembrane peptides is a fundamental biophysical process for toxin and viral actions. Polytheonamide B (pTB) is a potent cytotoxic peptide with a $\beta^{6.3}$-helical structure. Previous experimental studies revealed that the pTB inserts into the membrane in a vectorial fashion and forms a channel with its single molecular length long enough to span the membrane. Also, molecular dynamics simulation studies demonstrated that the pTB is prefolded in the aqueous solution. These are unique features of pTB since most of the peptide toxins form channels through oligomerization of transmembrane helices. Here, we performed all-atom molecular dynamics simulations to examine the dynamic mechanism of the vectorial insertion of pTB, providing underlying elementary processes of the membrane insertion of a prefolded single transmembrane peptide. We find that the insertion of pTB proceeds with only the local lateral compression of the membrane in three successive phases: "landing," "penetration," and "equilibration" phases. The free energy calculations using the replica-exchange umbrella sampling simulations present an energy cost of 4.3 kcal/mol at the membrane surface for the membrane insertion of pTB from bulk water. The trajectories of membrane insertion revealed that the insertion process can occur in two possible pathways, namely "trapped" and "untrapped" insertions: in some cases, pTB is trapped in the upper leaflet during the penetration phase. Our simulations demonstrated the importance of membrane anchoring by the hydrophobic N-terminal blocking group in the landing phase, leading to subsequent vectorial insertion.

STATEMENT OF SIGNIFICANCE

Polytheonamide B (pTB) is a channel-forming peptide toxin synthesized in bacteria. The peptide is hydrophobic with an unusual hydrophobic N-terminal blocking group, while the peptide is folded to β-helical structure in an aqueous solution. Spontaneous vectorial insertion of pTB into membrane has been demonstrated experimentally, and the mechanism underlying this process is examined here using all-atom molecular dynamics simulations and free energy calculations. This theoretical study revealed that anchoring by the N-terminal blocking group from aqueous solution to the membrane surface is crucial for the subsequent vectorial insertion. These findings serve as a framework for understanding the vectorial insertion of other peptides prefolded in aqueous solution.

INTRODUCTION

The peptide insertion into the cell membrane is crucial for toxin actions,[1] viral infections,[2] and antimicrobial defense.[3] While peptides like β-amyloid,[4] α-Synuclein,[5] and Influenza A M2[6] operate as channels through oligomer formation, other peptides like magainin,[7] alamethicin,[8] and melittin[8,9] deform the membrane substantially to form toroidal pores. Having rich hydrophobic residues, they are eventually settled in the membrane. However, toward the settlement, these peptides encounter a challenging membrane insertion process after approaching the membrane surface. Moreover, these peptides are inserted unidirectionally led by the preferred terminal, i.e., vectorial insertion, which secures the activity of the relevant peptides in the membrane: wrong orientation disrupts peptides' functionality in the membrane, such as to respond to the membrane electric field adequately. So far, studies of spontaneous membrane insertion have been performed using synthesized peptides.[10–13] Thermodynamic processes of spontaneous membrane insertion have been described with sequential processes: unfolded peptide in the bulk aqueous solution folds at the membrane interface, followed by membrane insertion.[10,12] However, these studies did not address the mechanism of vectorial insertion that most native peptides do.

Here, we applied the cytotoxic peptide, polytheonamide B (pTB), among other membrane-targeting peptides to understand the dynamic elementary processes of vectorial insertion. The 48-residue pTB is a cytotoxin obtained from the marine sponge *Theonella swinhoei*.[14–23] The potent cytotoxicity of pTB is related to its channel-forming activity across the target cell membrane by spontaneously inserting into the membrane.[15,18] The alternate D- and L-amino acids throughout the sequence allow the peptide to take a right-handed $\beta^{6.3}$-helical conformation, similar to the gramicidin A (gA) channel (see Fig. 1a).[24] Furthermore, the hydrophobicity of residues decreases gradually from the N-terminal to the C-terminal.[18] The long and short side chain – side chain

hydrogen bond strands outside the pore reinforce the stability of the long $\beta^{6.3}$-helix of pTB (see Fig. 1a).[25]

Structural features suggest that the pTB vectorially inserts into the membrane led by the hydrophobic N-terminal and stays in the membrane stably.[18,21,22,26,27] The highly hydrophobic N-terminal blocking group, 5,5-dimethyl-2-oxo-hexanoyl (Mhe, see Fig. 1a), is thought to anchor pTB into the target cell membrane.[18] The 40 Å long pTB can readily span the membrane as a monomeric channel and allows the permeation of monovalent cations.[15,18,21,22] This is a unique feature of pTB since most of the peptide toxins form channels through oligomerization of transmembrane helices with amphipathic nature. Molecular dynamics simulations have revealed that pTB is prefolded in the bulk aqueous solution.[23,25] Thus, pTB serves as a peptide showing the most straightforward process of the vectorial membrane insertion, and such a simple insertion process has not been studied before. Understanding this simple process provides elementary clues for more complicated vectorial membrane insertion processes, including hydrophobic membrane-spanning segments of membrane proteins. Here, we examine the vectorial insertion of pTB, to understand the underlying dynamic elementary processes of the membrane insertion of prefolded single transmembrane peptides.

Molecular dynamics (MD) simulation is a powerful tool that provides atomistic details for understanding the membrane insertion process of various peptides, although its utility is strongly dependent on the accessible time scales and the accuracy of the force fields used. In fact, the observation of membrane insertion of peptides is rather time-consuming using the conventional MD simulations, due to the presence of a finite energy barrier for the insertion. Consequently, most of the theoretical and computational studies on the membrane insertion of peptides are centered around the free energies of peptide insertion.[28–36]

The recent developments in the computational efficiency and the underlying force fields of MD simulations have made it possible to study the spontaneous membrane insertion of various peptides, such as antimicrobial peptides,[37–40] thermostable peptides,[10–13] pH low-insertion peptide (pHLIP),[41] first transmembrane α-helix of CXCR4,[42] cell-penetrating HIV-1 TAT peptide,[43] and synthetic WALP and TMX peptides.[44–47] The study using the thermostable peptides at a temperature of 80 ^{o}C reveals that the general pathways taken by membrane-inserting peptides consist of three phases: surface adsorption, interfacial folding, and folded transmembrane insertion.[10,12] The simulations using the α-helix of CXCR4 suggest that both the membrane insertion and the preferred orientation of the transmembrane peptides during the insertion are determined by competition and cooperation between hydrophobic and electrostatic interactions, although successful spontaneous insertion was not observed.[42] Despite these studies, the mechanism of the vectorial membrane insertion of prefolded single transmembrane peptides at room temperature is currently not fully understood.

In this study, the membrane insertion of pTB is examined using all-atom MD simulations. The free energy profiles of insertion are analyzed using the replica-exchange umbrella sampling (REUS) simulations. We find a free energy barrier of 4.3 kcal/mol located at the membrane surface for pTB to get inserted into the membrane from bulk water, which is arising from the entropic bottleneck. In between the global free energy maximum and minimum, there is a "shoulder" region corresponding to the trapping of pTB in the upper leaflet. The Voronoi tessellation analysis of the area per lipid (APL) suggests that the insertion of pTB causes only the local lateral compression of the membrane. On the other hand, the membrane thickness remained almost constant during the insertion because of small "hydrophobic mismatch."

To clarify the vectorial insertion mechanism, the membrane insertion pathways of pTB are investigated in detail using unconstrained MD simulations. Our simulations confirm the experimental observation of the spontaneous vectorial insertion of pTB into the membrane, with membrane anchoring by the hydrophobic N-terminal blocking group (Mhe).[18,20] The overall insertion process takes place in three successive phases: "landing," "penetration," and "equilibration" phases. The individual insertion process can occur in two possible pathways, namely "trapped" and "untrapped" insertions, according to whether or not pTB is trapped in the upper leaflet during the penetration phase. Being the first theoretical and computational study of the vectorial membrane insertion of a β-helical peptide, our results can provide variable insights to clarify the membrane insertion mechanism of other vectorially inserting prefolded single transmembrane peptides.

This paper is organized as follows. Section 2 describes the methods of system preparation and the simulation details. In Section 3, we present our simulation results and discuss the results using various analyses. Finally, conclusions are given in Section 4.

METHODS

In the present study, we examined the insertion of pTB into the POPC bilayer using all-atom MD simulations. The POPC bilayer was chosen for this study because of its similarity with the DPhPC bilayer used in the experiments of pTB,[18,21] and the length of the pTB channel roughly matches the thickness of a POPC bilayer. The force field parameters for the natural amino acids were taken from the AMBER ff14SB force field.[48] The parameters for the non-standard groups in pTB (Hva, Tle, Asm, Ham, Mgn, Mil, Mme, and Mhe) were taken from our previous work.[23] The TIP3P model was used for water molecules.[49] The POPC bilayer parameters were taken

from the Lipid14 force field.[50] The ions were modeled using the monovalent ion parameters developed by Joung and Cheatham.[51]

All MD simulations were performed at three-dimensional periodic boundary conditions using AMBER18 package.[52] The bonds involving hydrogen were constrained using the SHAKE algorithm,[53] enabling a time step of 2 fs. Long-range electrostatic interactions were taken into account using the particle mesh Ewald approach[54] with a real-space cutoff of 12 Å. For all simulations, the Langevin thermostat[55] with a collision frequency of $\gamma = 1.0$ ps^{-1} was used to maintain the temperature at the relevant experimental temperature of 303 K[50], and the isotropic Berendsen barostat[56] with a pressure relaxation time of $\tau = 1.0$ ps was used to maintain the pressure at 1 atm.

For the preparation of POPC bilayer, a fully hydrated POPC bilayer having 100 lipid molecules in each layer was first constructed using the CHARMM-GUI Membrane Builder.[57] The generated membrane patch had 58 Å thick hydration layer on each side, and 0.15 M CsCl salt concentration added to bulk water. The CsCl salt was chosen because of the high ionic conductivity of Cs^+ ions in the planar lipid bilayer experiments of the pTB channel.[18,21] The generated POPC bilayer was then undergone an energy minimization for 10000 steps, of which the first 5000 steps used the steepest descent method and the remaining steps used the conjugate gradient method.[58] This was followed by heating from 0 K to 303 K under the NVT conditions for 100 ps, and finally an equilibration run at the NPT conditions for 50 ns. The equilibration of the system was confirmed by comparing the average APL and membrane thickness, with those reported in the previous experimental and simulation studies.[50,59] The average APL and membrane thickness obtained are 65.6 $Å^2$ and 38.6 Å, respectively.

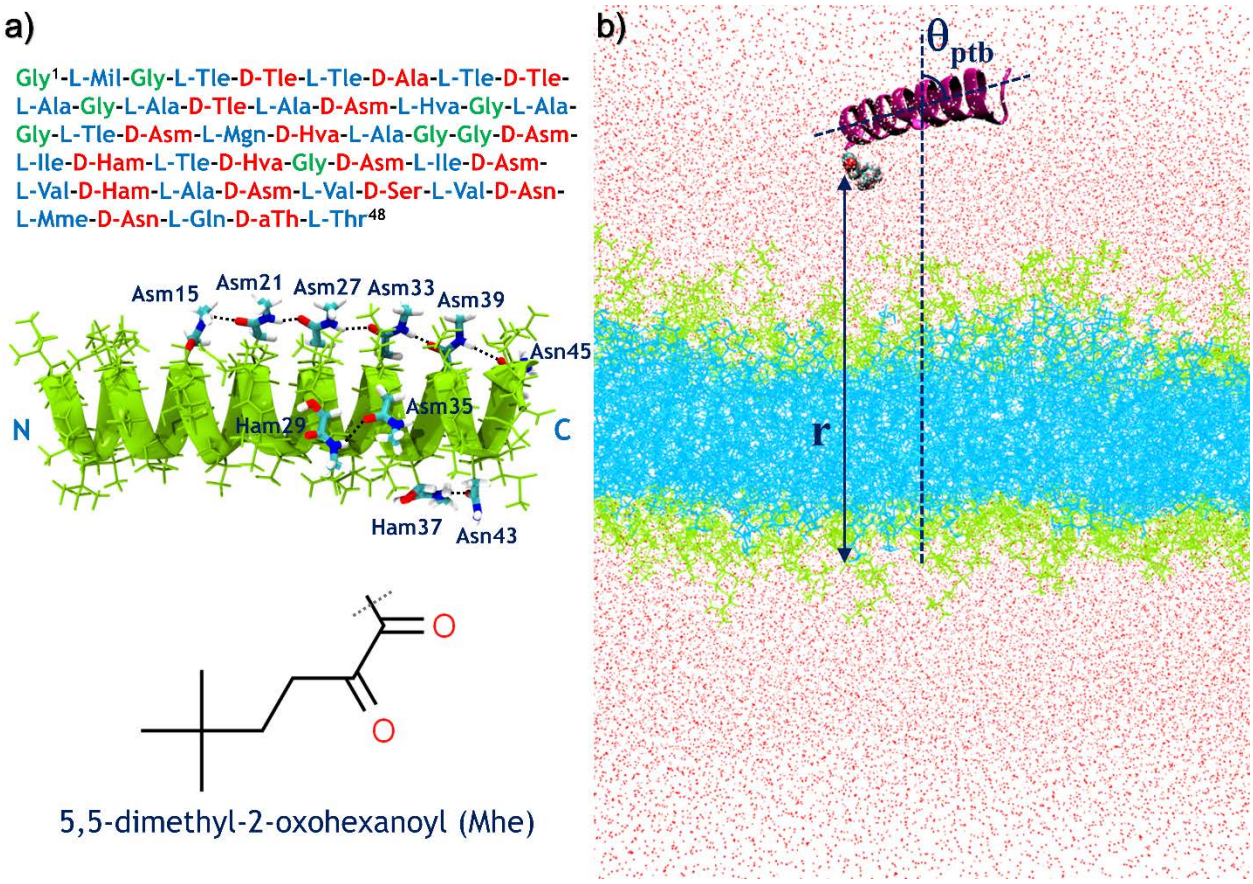

Figure 1: (a) Primary and tertiary structures of pTB, and structure of N-terminal blocking group (Mhe). In the primary structure, residues are numbered from the N-terminal to the C-terminal. The amino acid residues shown in green, red, and blue are Glycine, D-type, and L-type residues, respectively. There are eight types of unnatural amino acids in pTB: β-hydroxyvaline (Hva), *tert*-leucine (Tle), γ-N-methylasparagine (Asm), γ-N-methyl-*threo*-β-hydroxyasparagine (Ham), β-methylglutamine (Mgn), β-methylisoleucine (Mil), β,β-dimethylmethionine sulphoxide (Mme), and *allo*-threonine (aTh). The right-handed $\beta^{6.3}$-helical backbone of pTB is shown as a green ribbon and side chains as thin green stick models. The thick stick models represent the side chains of residues involved in the side chain – side chain hydrogen bonds, which are labeled with their residue numbers. The black dots indicate hydrogen bonds. **(b)** A snapshot image of the system under study. In the snapshot image, pTB is represented as a magenta ribbon model with Mhe shown as a van der Waals sphere model, and the membrane as thin stick models with lipid head and tail groups in light-green and cyan colors, respectively. Water and ions are represented as points. The definitions of the reaction coordinate, $\boldsymbol{r}$, and the tilt angle, $\boldsymbol{\theta_{ptb}}$, are also indicated in the snapshot image.

Subsequently, the equilibrium structure of pTB in water, taken from our previous work,[23] was inserted into bulk water. The water molecules that overlap with the inserted pTB molecule were then removed. One Cs^+ ion was added for neutralizing the net charge of the deprotonated C-terminal of pTB. The final system was comprised of one pTB molecule, 200 POPC lipid

molecules, 23126 water molecules, 64 Cs^+ ions and 63 Cl^- ions, resulting in a total of 97032 atoms. The combined system was then undergone an energy minimization for 10000 steps, of which the first 5000 steps used the steepest descent method and the remaining steps used the conjugate gradient method.[58] This was followed by an equilibration run at the NPT conditions for 50 ns. The simulation cell dimensions of the fully equilibrated system were ~ 81 × ~ 81 × ~ 146 $Å^3$, and this system was used to initialize the subsequent free energy calculations. A snapshot image of the system under study is given in Fig. 1b. In all the simulations in this study, almost no deformation from the rectangular shape of the equilibrium system was observed.

The one-dimensional potential of mean force (1D-PMF) profile of insertion was calculated from the REUS simulations.[60,61] The reaction coordinate (RC) is taken to be the distance along the membrane normal, between the C atom at the center of the *tert*-butyl part of the N-terminal blocking group (Mhe) and the center of mass (COM) of P atoms of the headgroups in the lower leaflet (see Fig. 1b). The bilayer side having the shortest distance from pTB is termed as the upper leaflet and the other side is termed as the lower leaflet hereafter. The membrane normal is defined as the vector pointing from the COM of upper leaflet to that of lower leaflet. The RC was varied from 80 to 0 Å with a window spacing of 1.0 Å, resulting in a total of 81 windows, using harmonic biasing potential with a force constant of 1.0 kcal mol^{-1} $Å^{-2}$. The replicas for individual windows were well equilibrated for 1 μs at the NPT conditions prior to the REUS simulations. At each window, the system was undergone 3 μs REUS run at the NPT conditions with trajectory data recorded every 10 ps. For better statistics, the RC was recorded every 100 fs from the REUS simulations, resulting in a total of 30 million RC values for each window. The one-dimensional weighted histogram analysis method (1D-WHAM)[62–64] was used to construct the 1D-PMF profile from the RC data collected from the REUS simulations.

The two-dimensional potential of mean force (2D-PMF) profile was then constructed from the 1D REUS simulation data by introducing θ_{ptb} as the second RC, using the two-dimensional weighted histogram analysis method (2D-WHAM)[63,64] where the biasing function for the second RC is presumed to have a zero force constant. The θ_{ptb} is the angle pTB makes with the bilayer normal (see Fig. 1b). In this paper, pTB is defined as the vector pointing from the COM of the first six Cα atoms at the C-terminal to that at the N-terminal.

For observing the vectorial insertion of pTB into the POPC bilayer, we carried out 30 long unbiased MD simulations (each for > 1.5 μs) under the NPT conditions from different starting points farther than the transition state (TS) at the 1D-PMF profile. The initial configurations for the unbiased simulations were taken from the REUS simulations. The unbiased trajectory data was recorded every 10 ps.

The standard CPPTRAJ analysis routines[65] and in-house written scripts were applied for the analyses. The Voronoi tessellation of membrane surface was constructed using the APL@Voro program.[66] All snapshot images and movies from the simulations were generated using the Visual Molecular Dynamics (VMD) package.[67]

RESULTS AND DISCUSSIONS

We first discuss the results on the free energy profile of membrane insertion, followed by the results on the spontaneous vectorial insertion of pTB into the membrane, and finally the footprints of membrane insertion.

Free Energy Profile of Membrane Insertion

Figure 2a shows the 1D-PMF profile of insertion. Standard deviations of the 1D-PMF profile are calculated by dividing the simulation data into 6 blocks, using 1D-WHAM to calculate a 1D-PMF from the data in each block, and then determining the statistical uncertainty from the variance of the 1D-PMFs. The pTB moved from 80 to 0 Å along the RC, r. The free energy change for r varying from 80 to 60 Å is 0.8 kcal/mol (1.3 k_BT, where k_B and T are the Boltzmann constant and the temperature of the system, respectively), since the interaction between pTB and the membrane is very small. This corresponds to the "free-floating region" ($r \geq 60$ Å) of the 2D-PMF profile shown in Fig. 2b, where the free energy contours along the tilt angle are broad, indicating the large orientational freedom of pTB due to the absence of strong interactions with the membrane.

The free energy shows a gradual increase from 60 Å as pTB moves toward the membrane surface (~ 42.5 Å), which corresponds to the "membrane sensing region" ($42.5 \leq r < 60$ Å) of the 2D-PMF profile. In the membrane sensing region, larger tilt angles are restricted as pTB starts to feel the presence of membrane, thereby making the width of the free energy contours along the tilt angle bit smaller than those in the free-floating region. The distribution of θ_{ptb} is narrowed in this region due to the asymmetry in the pTB structure, i.e., the hydrophobicity of residues decreases gradually from the N-terminal to the C-terminal.[18] As a result, the N-terminal tends to be closer to the membrane surface than the C-terminal does. It is found that the highly hydrophobic N-terminal blocking group (Mhe) anchors the membrane approach of pTB from bulk water.

This membrane anchoring by Mhe is driven by the unfavorable interactions of the N-terminal in bulk water, and is important for the vectorial insertion of pTB found in the experimental studies.[18] The vectorial insertion of peptide, in which the peptide is inserted into the

membrane in only one direction, is a result of the feature called the “axial amphipathicity”.[18] Therefore, it is important for the peptide to have membrane anchoring by the preferred terminal in order for the vectorial insertion into the membrane, as found in a previous study for the first transmembrane α-helix of CXCR4 where the C-terminal is found to anchor the membrane insertion process.[42]

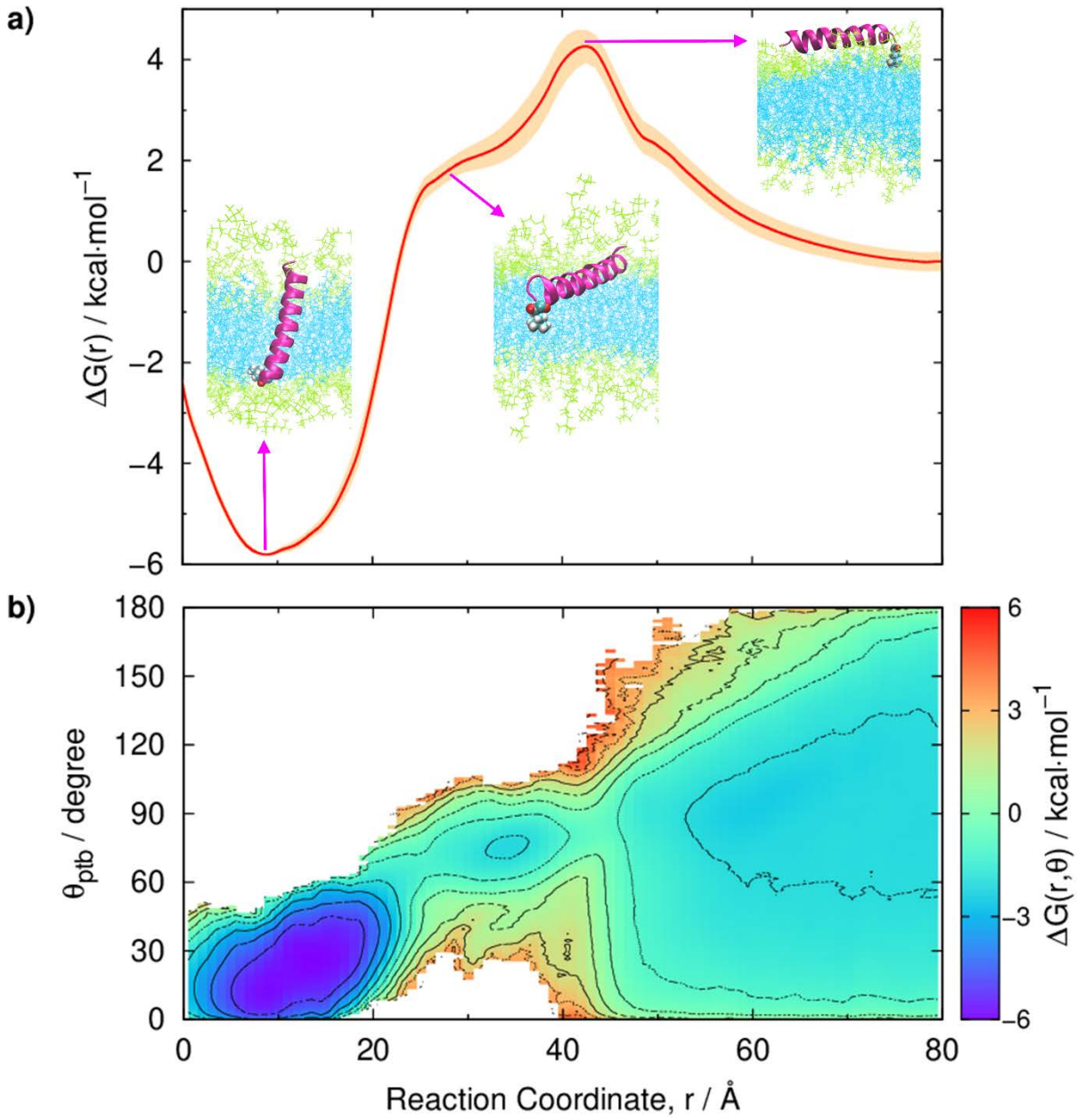

Figure 2: (a) One-dimensional free energy profile as a function of the reaction coordinate, $\boldsymbol{r}$. Standard deviations of the free energies are represented by shaded regions. Snapshot images corresponding to the transition state, shoulder region, and global minimum are shown in the inset. In the snapshot images, pTB is represented as a magenta ribbon model with Mhe shown as a van der Waals sphere model, and the membrane as thin stick models with lipid head and tail groups in light-green and cyan colors, respectively. For clarity, water and ions are not shown in the snapshot images. **(b)** Two-dimensional free energy surface as a function of the reaction coordinate, $\boldsymbol{r}$, and the tilt angle, $\boldsymbol{\theta_{ptb}}$.

Then, the free energy barrier of 4.3 kcal/mol (~ 7.2 k_BT) is found at 42.5 Å, which is the TS. The pTB lay on the surface of the upper leaflet with an average tilt angle of 78.6±11.8^0 at the TS (see inset of Fig. 2a). The region below the TS corresponds to the "membrane penetrating region" ($r < 42.5$ Å) of the 2D-PMF profile. In the membrane penetrating region, the contours become narrow as pTB penetrates into the membrane, which is due to the restricted orientational freedom of pTB arising from the strong interactions with the membrane. After crossing the barrier, the free energy gradually decreases. It is noted that the membrane penetration of pTB occurs specifically with the N-terminal and is driven by the hydrophobic interactions between the N-terminal and the tailgroups of the membrane, consistent with the experimental results.[18]

The pTB then reaches a "shoulder region" of 10 Å length from 35 to 25 Å, which corresponds to the trapping of pTB in the upper leaflet (see inset of Fig. 2a). Due to the asymmetry in the structure of pTB, the shoulder region is stabilized by the hydrophilic interactions between the C-terminal and the headgroups, and the hydrophobic interactions between the N-terminal and the tailgroups of the upper leaflet. After the shoulder region, the free energy decreases steeply and reaches the global minimum at 8.5 Å with a stabilization of -5.8 kcal/mol relative to the solution phase. At the global free energy minimum, the pTB was fully inserted with the N-terminal residing just below the headgroup region of the lower leaflet and the C-terminal touching the membrane surface of the upper leaflet (see inset of Fig. 2a), as found in our previous work.[23] The average θ_{ptb} value at the global free energy minimum is 16.9±8.1^0. The $\beta^{6.3}$-helix of pTB with side chain – side chain hydrogen bond strands outside the pore remained intact throughout the insertion process. Finally, the free energy starts to increase again as pTB penetrates further from the global minimum toward the headgroup region of the lower leaflet. For the previously studied spontaneously inserting peptides, membrane insertion is

preceded by interfacial folding of peptides. Therefore, there exists a free energy well at the membrane surface due to folding, followed by a free energy barrier for the membrane insertion of the folded peptide.[10,12,35] On the other hand, pTB is highly hydrophobic and prefolded in the solution phase, resulting in a free energy profile different from other peptides.

The elastic energy arising from the stretching/compressing of the bilayer area in the upper leaflet can be approximated by $\frac{1}{2}K_A n_L A_0 \left(\frac{A-A_0}{A_0}\right)^2$, where A_0, A, n_L, and K_A are the equilibrium APL, deformed APL, number of lipids in each leaflet, and bilayer area compressibility modulus, respectively.[68] The K_A can be obtained from the equilibrium fluctuations of the APL as $\frac{k_B T<A_0>}{n_L<\delta {A_0}^2>}$.[68,69] The elastic energy contribution from the area deformation of the bilayer is 2.9 kcal/mol, with K_A having a value of 257.6 mN/m. The calculated K_A value is in good agreement with the experimental value.[69] Thus, the observed free energy barrier and bilayer area deformation energy might be slightly lowered by performing simulations with either NPT ensemble with semi-isotropic pressure control or NPγT ensemble.

The free energy barrier obtained with POPC bilayer for the membrane insertion of the α-helical antimicrobial peptide, melittin, is 13.2 kcal/mol,[35] while that for a closed and pristine 5 nm long single-walled carbon nanotube is 4.9 kcal/mol.[70] The high free energy barrier associated with the membrane insertion of melittin can be seen as a result of the large hydration of melittin arising from the presence of multiple charged residues. On the other hand, the small hydration in the case of pristine carbon nanotube results in the small free energy barrier for its membrane insertion.

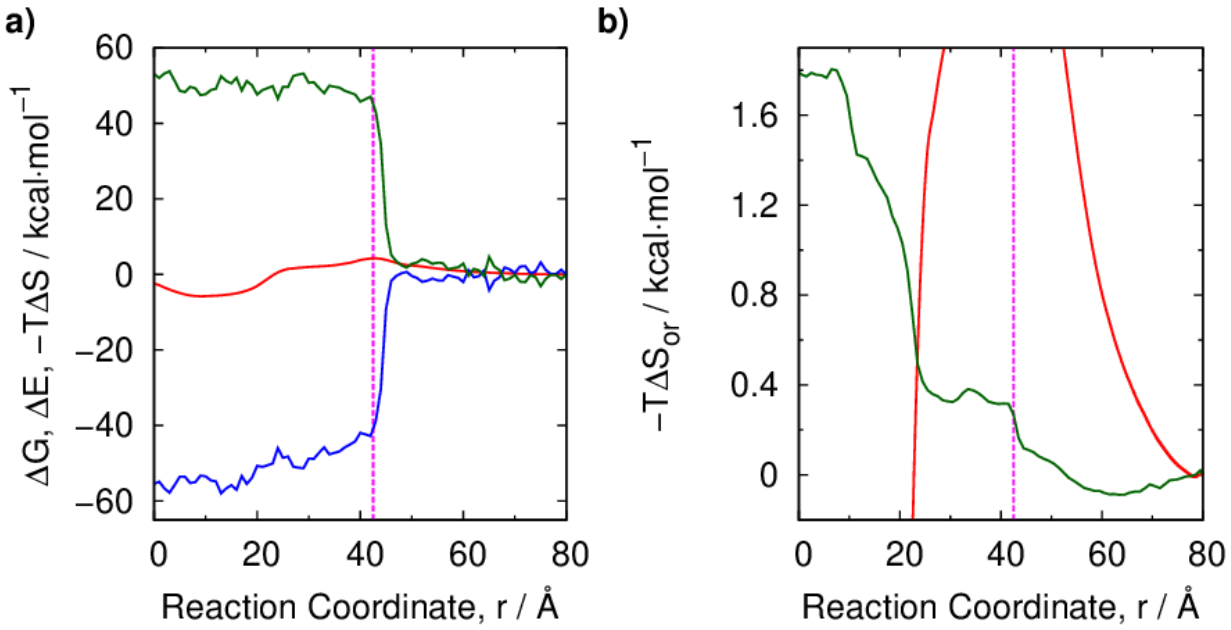

Figure 3: (a) Free energy (ΔG, red), energy (ΔE, blue), and entropy (-TΔS, dark-green) as a function of the reaction coordinate, $\boldsymbol{r}$. **(b)** Orientational entropy (-$T\Delta S_{or}$, dark-green) as a function of the reaction coordinate, $\boldsymbol{r}$. Free energy (ΔG, red) is also shown for reference. In both the figures, $\boldsymbol{r} = 42.5$ Å (transition state) is marked with pink dashed lines.

The average energy (ΔE) and entropy ($-T\Delta S$) along r are given in Fig. 3a. The average energies are calculated from the REUS simulation data using the equation $< E(r)e^{\beta U(r)} > / < e^{\beta U(r)} >$, where $E(r)$ and $U(r)$ are respectively the total potential energy of the system and the umbrella potential at r, $\beta = 1/k_B T$, and $< \cdots >$ denotes ensemble average. The total potential energy is defined as $E = E_{ptb} + E_{popc} + E_{water} + E_{ion} + E_{ptb-popc} + E_{ptb-water} + E_{ptb-ion} + E_{popc-water} + E_{popc-ion} + E_{water-ion}$, where the subscripts specify the various components of the total potential energy, and these components along r are given in Figs. S1-S3 of Supporting Information. The standard deviations of the total potential energy of the system are large because of the slow convergence of the total energy and are therefore not shown in Fig. 3a. The entropy ($-T\Delta S$) is evaluated as $-T\Delta S = \Delta G - \Delta E - P\Delta V$. It is found that the pressure-volume term ($P\Delta V$) is negligibly small. As seen in Fig. 3a, both the energy and

entropic terms are rather flat when $r \geq 46$ Å and then they gradually change as pTB moves further toward the TS resulting in a barrier (no barrier) in the entropy (energy) profile at 42.5 Å. Therefore, it is now clear that the free energy barrier at 42.5 Å arises from the "entropic bottleneck" rather than enthalpic term. After crossing the TS, ΔE slightly decreases, whereas $-T\Delta S$ is rather flat compared with ΔE.

As seen in Fig. 2b, the restriction of the orientation of pTB with respect to the membrane normal, i.e., the restriction of θ_{ptb}, as r varies from 80 to 0 Å leads to a decrease in orientational entropy. The orientational entropy along r can be evaluated by $S_{or}(r) = -k_B \int_0^{\pi} \rho(r, \theta_{ptb}) \ln \rho(r, \theta_{ptb}) \sin \theta_{ptb} \, d\theta_{ptb}$, where $\rho(r, \theta_{ptb})$ is the 2D probability density of r and θ_{ptb}.[71] This orientational entropic contribution, $-TS_{or}(r)$, to the observed free energy barrier is ~ 0.4 kcal/mol as seen in Fig. 3b, which is only 9 % of the total barrier. Note that the entropic contribution estimated here is not the overall entropic contribution to the free energy barrier, instead the contribution just from the tilt angle of pTB. Even though the calculation of individual entropy components is difficult for a complex system like the present system, the loss of entropy arising from the change of hydration upon the membrane approach of pTB is considered to be responsible for the entropic bottleneck in the free energy profile.

The analyses of various energy components given in Figs. S1-S3 of Supporting Information led to the following conclusions. The energy change associated with the insertion is defined as the change in energy when pTB moves from 80 to 9 Å along r ($E_{9\,\text{Å}} - E_{80\,\text{Å}}$). The N- and C-terminals of pTB show fluctuations in bulk water because the surrounding water molecules can easily break the backbone hydrogen bonds near the terminals by forming stable hydrogen bonds with the backbone atoms, as found in our previous work.[23] These fluctuations

are largely suppressed in the process of going from bulk water to the hydrophobic core of the membrane, resulting in an energy stabilization of -46.9 kcal/mol in E_{ptb}. On the other hand, E_{popc} has an energy destabilization of 47.1 kcal/mol in the process, arising from the destabilization of the bilayer structure caused by the insertion of pTB. There is a large destabilization of 423.3 kcal/mol in $E_{ptb-water}$ as pTB loses its solvation structure in bulk water for getting inserted into the membrane. The loss of solvation of pTB by water molecules in bulk water, in turn, causes an increase in water-water interactions, resulting in a stabilization of -300.6 kcal/mol in E_{water}. When pTB gets fully inserted into the membrane, $E_{ptb-popc}$ has a stabilization of -360.3 kcal/mol due to the maximization of pTB-membrane interactions. Also, there is a gradual decrease in the membrane-water interactions as pTB becomes closer to the membrane surface, due to the displacement of many water molecules which are closer to the membrane surface by pTB, resulting in a destabilization of 193 kcal/mol in $E_{popc-water}$. No such significant changes are seen in the remaining energy components $E_{ptb-ion}$, $E_{popc-ion}$, $E_{water-ion}$, and E_{ion} as pTB moves from bulk water to the hydrophobic core of the membrane. It is now clear that the global free energy minimum is mainly obtained by the stabilization of both water-water and pTB-membrane interactions. Therefore, it is found that the stabilization of $E_{ptb} + E_{ptb-popc} + E_{water}$ in going from bulk water to the hydrophobic core of the membrane is partially canceled with the destabilization of $E_{popc} + E_{ptb-water} + E_{popc-water}$, giving rise to a stabilization of -53.3 kcal/mol in the total potential energy E.

Also, the free energy increase as pTB further inserts from the global minimum is due to the decrease of both pTB-water and membrane-water interactions. As pTB moves to the lower leaflet, the number of water molecules in contact with the pTB and the membrane surfaces

decreases because the terminals of pTB displace the water molecules near the respective surfaces, resulting in the increase of $E_{ptb-water}$ and $E_{popc-water}$ components.

Spontaneous Vectorial Membrane Insertion

To reveal the molecular processes in the membrane insertion of pTB behind the free energy profile, we carried out 30 long unbiased MD simulations from $r > 42.5$ Å as described in the Methods section. A total of 8 successful spontaneous membrane insertion trajectories are obtained out of the 30 tries. In all the unsuccessful trajectories, pTB occasionally attempts to penetrate the membrane surface, but never succeeds, and then moves back to the water phase. The analyses of the 8 successful insertion trajectories clearly show two distinct insertion pathways, which are termed as "trapped" and "untrapped" insertions hereafter (Figs. 4 and 5, Videos S1 and S2). In the trapped insertion, the pTB gets trapped in the upper leaflet for several hundred nanoseconds (see Fig. 5). The period for which the pTB got trapped in the upper leaflet is called the "quiescent period" during the trapped insertion. The quiescent period is in the range of ~ 250-450 ns for the 3 trapped trajectories we obtained. On the other hand, there occurs no such trapping in the untrapped insertion (see Fig. 4). The remaining 6 insertion trajectories are shown in Figs. S4-S9 of Supporting Information. Out of the 8 independent insertion trajectories, untrapped insertion occurs for 5 trajectories and trapped insertion occurs for the remaining 3 trajectories. Therefore, it is conceivable that untrapped insertion is the dominant insertion pathway for pTB.

Irrespective of the type of insertion pathway, the insertion process can be described by three successive phases: "landing," "penetration," and "equilibration" phases. As time passes, the pTB which is initially placed in bulk water lands on the surface of the upper leaflet, thereby

reaching the TS of the 1D-PMF profile. This is the “landing” phase, in which the pTB takes a lower tilt angle prior to the membrane “penetration” phase, and its duration is in the range of 0.1-1.2 μs depending on the trajectory. The penetration phase is followed by an “equilibration” phase, in which the pTB embedded membrane system equilibrates. It is noted that the pTB could penetrate only till the head/tail interface of the lower leaflet ($r \approx 8.5$ Å, the global free energy minimum) in all the insertion trajectories, as expected from the 1D-PMF profile.

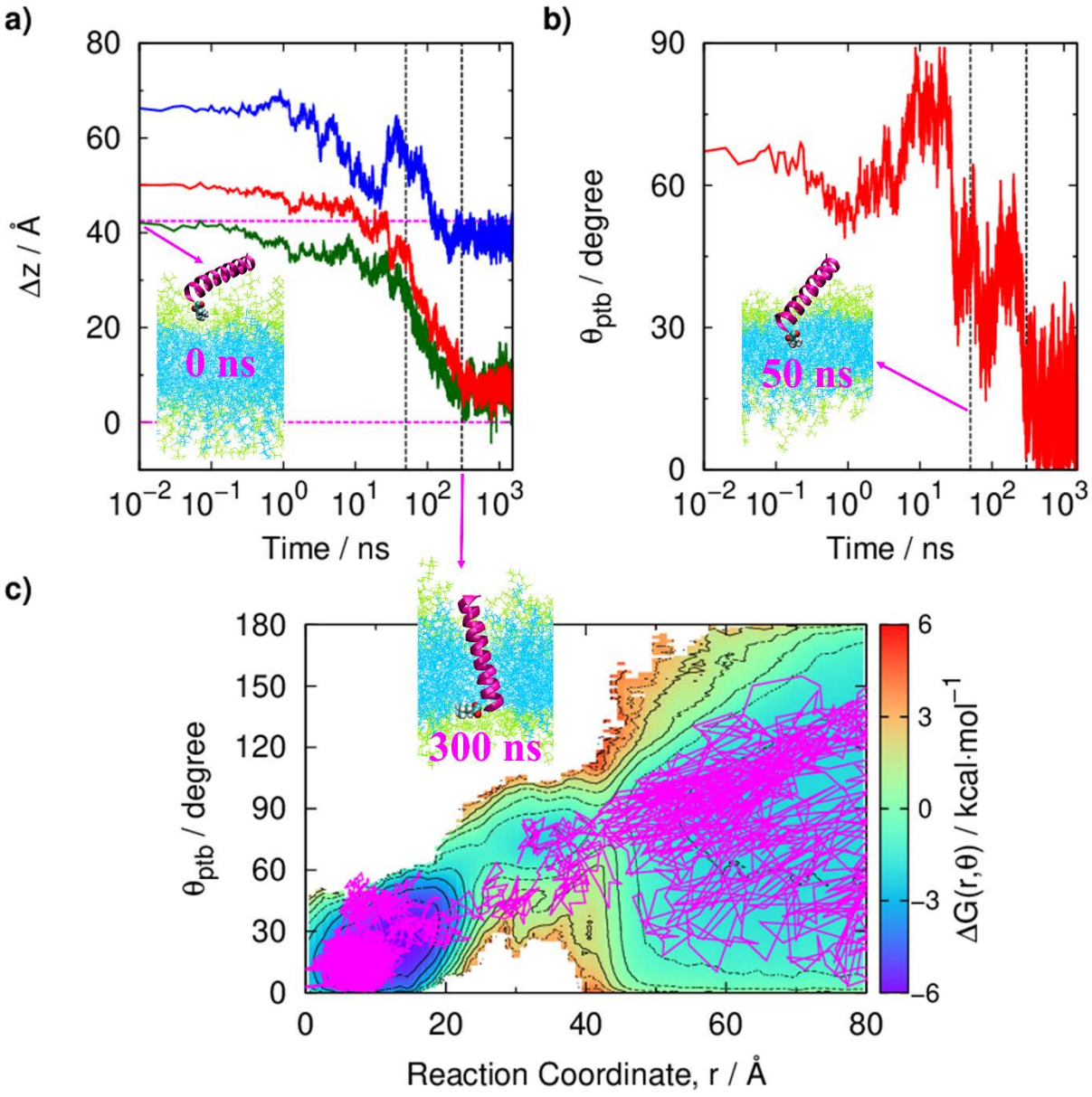

Figure 4: Characteristic example of an untrapped insertion of pTB. Time courses of **(a)** reaction coordinate, $\boldsymbol{r}$ (dark-green), z-distances of the N- (red) and C- (blue) terminals from the membrane surface of the lower leaflet, and **(b)** tilt angle, $\boldsymbol{\theta_{ptb}}$, during insertion. **(c)** Mapping of ($\boldsymbol{r}$, $\boldsymbol{\theta_{ptb}}$) values on the 2D-PMF profile using pink lines. In the top left figure, the transition state ($\boldsymbol{\Delta z} = 42.5$ Å) and the membrane surface of the lower leaflet ($\boldsymbol{\Delta z} = 0$ Å) are marked by pink dashed lines. Characteristic times 50 and 300 ns are marked with black dashed lines. Snapshot images at 0, 50, and 300 ns are also shown. In the snapshot images, pTB is represented as a magenta ribbon model with Mhe shown as a van der Waals sphere model, and the membrane as thin stick models with lipid head and tail groups in light-green and cyan colors, respectively. For clarity, water and ions are not shown in the snapshot images.

The insertion pathways are analyzed below in terms of the time courses of the RC (r), the z-distances of the N- and C-terminals from the membrane surface of the lower leaflet, and the tilt angle (θ_{ptb}). The N- and C-terminals are defined as the COMs of the first six Cα atoms at the respective terminals. In addition, the (r, θ_{ptb}) values are projected onto the 2D-PMF profile. All the insertion trajectories shown in this paper are time-shifted trajectories such that r is at the TS (42.5 Å) at t = 0 ns. That means that the time evolution of pTB before finally crossing the TS (for $r > 42.5$ Å), corresponding to the "landing" phase, is not shown in the time-course profiles. On the other hand, the (r, θ_{ptb}) mapping on the 2D-PMF surface is done using the whole insertion trajectory ($0 \leq r \leq 80$ Å).

First, we examine the untrapped membrane insertion of pTB. A characteristic example of an untrapped insertion is shown in Fig. 4. The "penetration" phase starts as pTB begins to penetrate the membrane led by the highly hydrophobic N-terminal blocking group (Mhe), with a tilt angle of 67^0 taken during the "landing phase". The penetration phase is a two-step process: the first and second steps represent the initial penetration of ~ 15 Å long region of the upper leaflet (~ $25 < r < 42.5$ Å) and the subsequent penetration of ~ 20 Å long region until pTB reaches the head/tail interface of the lower leaflet (~ $8.5 < r <$ ~ 25 Å), respectively. As seen in Fig. 4a, the pTB completes the first step of the penetration phase in ~ 50 ns when r reaches ~ 25 Å with a tilt angle of ~ 45^0. As pTB penetrates deeper into the hydrophobic core of the membrane, the tilt angle gradually changes to lower values and reaches a value of ~ 15^0 when pTB is fully inserted into the membrane at t = 300 ns. The duration of the second step of the penetration phase is ~ 250 ns in this example. The penetration phase is followed by an "equilibration" phase. It is noted that the periods of the three phases strongly depend on the

trajectory. Fig. 4c shows that the untrapped insertion process in this example almost follows the minimum energy path of the 2D-PMF surface.

Next, we examine the trapped membrane insertion of pTB. A characteristic example of a trapped insertion of pTB is shown in Fig. 5. After the initial "landing" phase, the pTB starts penetrating the membrane led by Mhe with a tilt angle of 73^0. The Mhe reaches at r = ~ 25 Å in ~ 220 ns, with a tilt angle of ~ 60^0, corresponding to the first step of the "penetration" phase. As seen in Fig. 5a, the N-terminal was not able to move much from there and stayed there for ~ 400 ns before penetrating into the lower leaflet, i.e., the pTB got trapped in the upper leaflet for the "quiescent period" of ~ 400 ns (see inset of Fig. 5b). The trapping occurs because the C-terminal tries to go deep inside the headgroup region of the upper leaflet in the meantime, instead of staying near the surface of the upper leaflet as in the case of untrapped insertion trajectories. This corresponds to the "shoulder region" of the 1D-PMF profile, and is a result of the stabilization of the hydrophilic and hydrophobic interactions between the terminals of pTB and the head-tail groups of the upper leaflet. A trapped insertion can be distinguished from the untrapped one by the distribution of large tilt angles in the shoulder region, as highlighted in Fig. 5c.

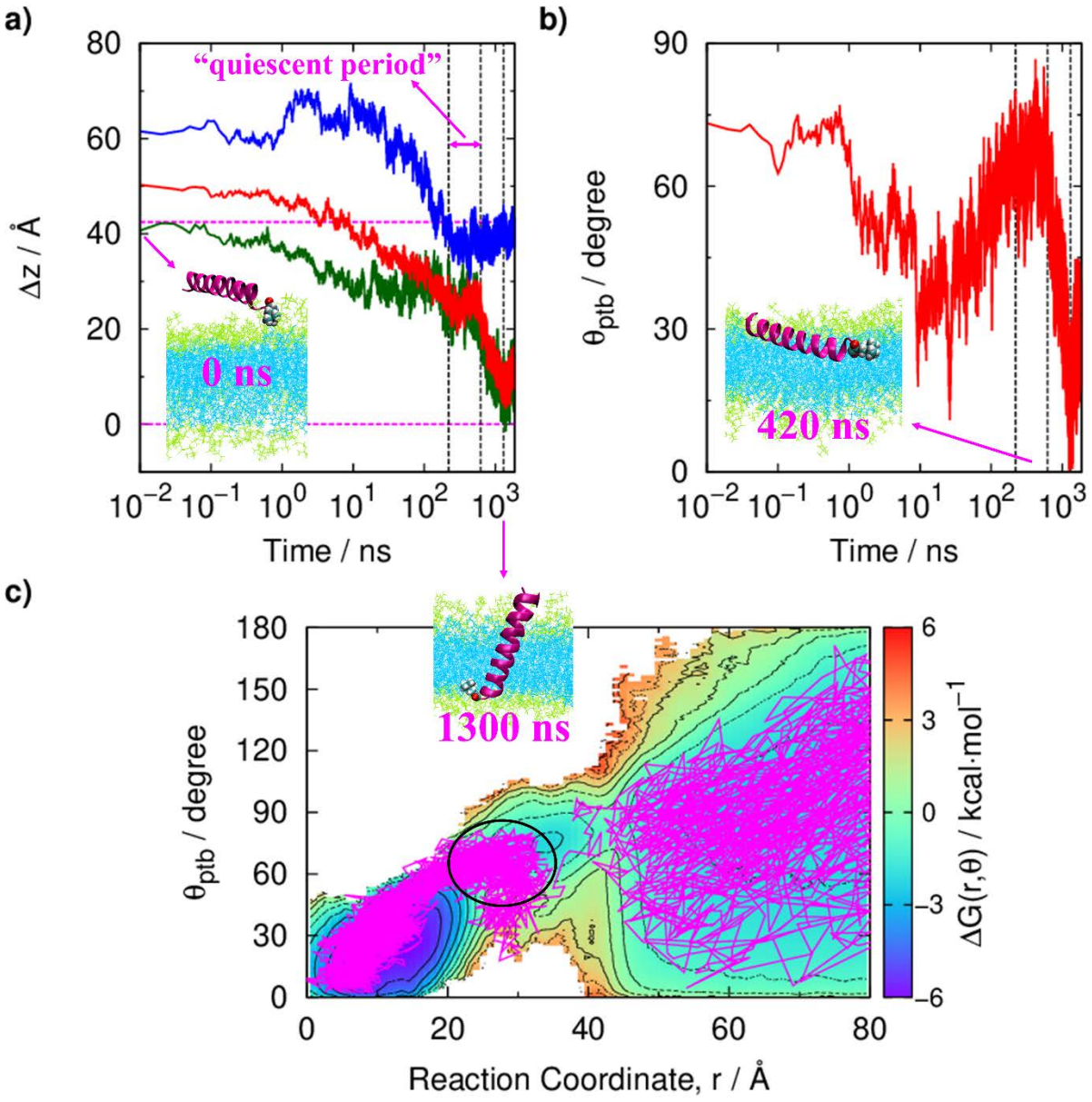

Figure 5: Characteristic example of a trapped insertion of pTB. Time courses of **(a)** reaction coordinate, $\boldsymbol{r}$ (dark-green), z-distances of the N- (red) and C- (blue) terminals from the membrane surface of the lower leaflet, and **(b)** tilt angle, $\boldsymbol{\theta_{ptb}}$, during insertion. **(c)** Mapping of ($\boldsymbol{r}$, $\boldsymbol{\theta_{ptb}}$) values on the 2D-PMF profile using pink lines. In the top left figure, the transition state ($\boldsymbol{\Delta z} = 42.5$ Å) and the membrane surface of the lower leaflet ($\boldsymbol{\Delta z} = 0$ Å) are marked by pink dashed lines. Characteristic times 220, 620, and 1300 ns are marked with black dashed lines. Snapshot images at 0, 420, and 1300 ns are also shown. In the snapshot images, pTB is represented as a magenta ribbon model with Mhe shown as a van der Waals sphere model, and the membrane as thin stick models with lipid head and tail groups in light-green and cyan colors, respectively. For clarity, water and ions are not shown in the snapshot images. The "quiescent period" during the trapped insertion is highlighted in the top left figure, and the evolution of ($\boldsymbol{r}$, $\boldsymbol{\theta_{ptb}}$) during the quiescent period is marked with a black oval in the bottom figure.

When the C-terminal is closer to the surface of the upper leaflet again, the pTB starts the second step of the penetration phase at t = 620 ns with a tilt angle of ~ 60^0. As seen in Fig. 5a, Mhe paves the way for the further penetration of pTB when restarting the insertion after the quiescent period. Finally, the pTB gets fully inserted into the membrane at t = 1300 ns with a tilt angle of ~ 15^0. The duration of the second step of the penetration phase is ~ 680 ns. Due to the trapping of pTB in the upper leaflet, the penetration phase took much longer time than that of the untrapped insertion. This was followed by an "equilibration" phase. Interestingly, the trapped insertion process in this example also almost follows the minimum energy path of the 2D-PMF surface, as seen in Fig. 5c.

The "surface adsorbed" phase seen in the spontaneous insertion of thermostable peptides[10,12], resulting from the interfacial folding, is not observed in the case of pTB because the peptide is prefolded in the aqueous solution and the N-terminal is highly hydrophobic. That's the reason the 1D-PMF profile has the TS at the membrane surface instead of a free energy well. For the highly hydrophobic N-terminal of pTB, staying inside the hydrophobic core of the membrane is energetically more favorable than staying at the surface. To maximize the interaction of pTB with the membrane, the N-terminal stays at the head/tail interface of the lower leaflet while the C-terminal stays at the surface of the upper leaflet in the fully membrane inserted state. Note that the trapped state found in the insertion of pTB is not a surface adsorbed phase as the N-terminal is already buried inside the hydrophobic core of the upper leaflet.

Different from the membrane insertion of pTB, the penetration phase is followed by a "sliding" phase in the insertion pathway for the membrane insertion of carbon nanotubes.[70] The sliding phase, where the carbon nanotube slides along its axis deeper into the hydrophobic core of the membrane, is due to the lack of strong interactions of the rather hydrophobic carbon

nanotube with the hydrophilic headgroups of the membrane. On the other hand, the membrane insertion of pTB is a result of the strong interactions of pTB with both the head and tail groups of the membrane, arising from the structural asymmetry of pTB. As a result, the sliding phase is not observed in the insertion of pTB.

In both trapped and untrapped insertions, the pore of pTB allows the water molecules to permeate through the channel in a single-file fashion, as found in our previous study.[23] It is found that the water column inside the pTB is carried during the membrane penetration process, and is connected to bulk water from the C-terminal side as the penetration occurs with the N-terminal side. Once the pTB is fully inserted into the membrane, the water column near the N-terminal side also connects to bulk water from the other side. A similar mechanism was recently reported for the gramicidin A (gA) dimerization process to form the gA channel inside the membrane.[72] The water columns inside the two gA monomers join at the membrane center and connect to bulk water from the other two terminals during the channel formation process.

Footprints of Membrane Insertion

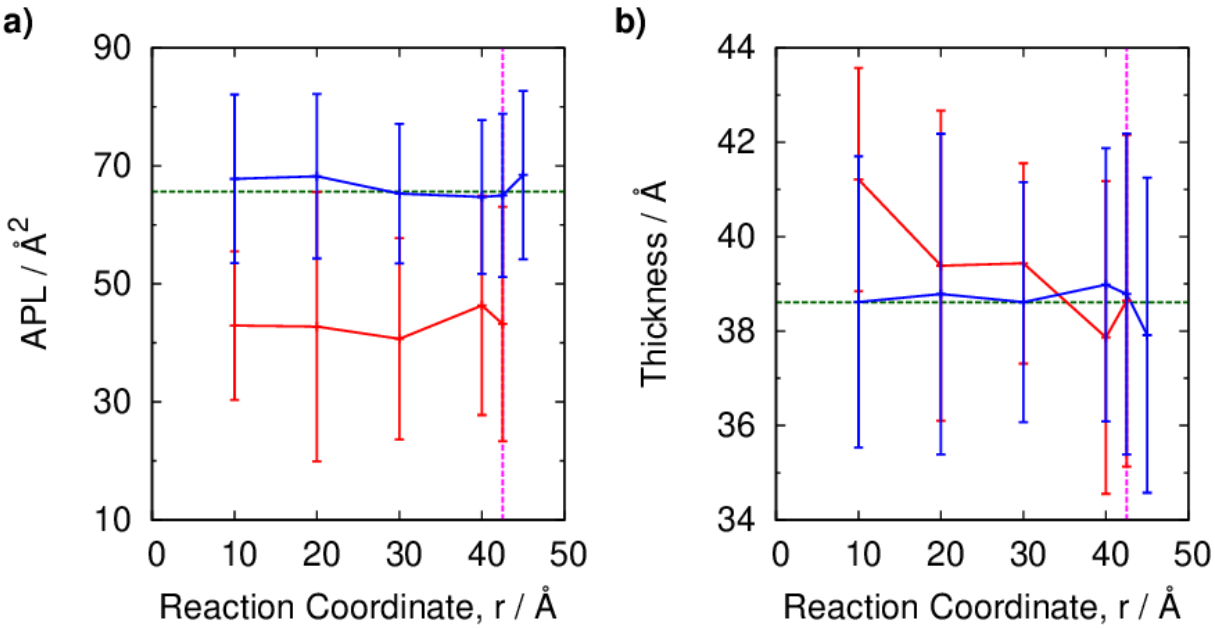

Figure 6: (a) Area per lipid (APL) and **(b)** membrane thickness for neighboring (red) and non-neighboring (blue) lipids as a function of the reaction coordinate, $\boldsymbol{r}$. Standard deviations are shown as error bars. The equilibrium values before the insertion of pTB are marked with dark-green dashed lines. In the figures, $\boldsymbol{r}$ = 42.5 Å (transition state) is indicated with pink dashed lines.

To characterize the perturbation of the bilayer during the insertion of pTB, we examined the average APL and membrane thickness for r = 45, 42.5, 40, 30, 20, and 10 Å at their most probable angles, using the REUS simulation data. We first analyzed the Voronoi cells associated with the APL of lipids in the upper leaflet. The surface of the upper leaflet is chosen for the Voronoi analysis because the pTB did not cross the head/tail interface of the lower leaflet during insertion. The Voronoi polyhedra are constructed using the P atoms of lipid headgroups in the upper leaflet. The equilibrium APL and membrane thickness before the insertion are 65.6 Å^2 and 38.6 Å, respectively. The average APL and thickness of "neighboring" and "non-neighboring" lipids at characteristic r values are shown in Fig. 6. Lipids in the first lipid shell around pTB are referred to as "neighboring" lipids and the rest as "non-neighboring" lipids. The Voronoi tessellations of the membrane surface at characteristic r values are shown in Fig. 7.

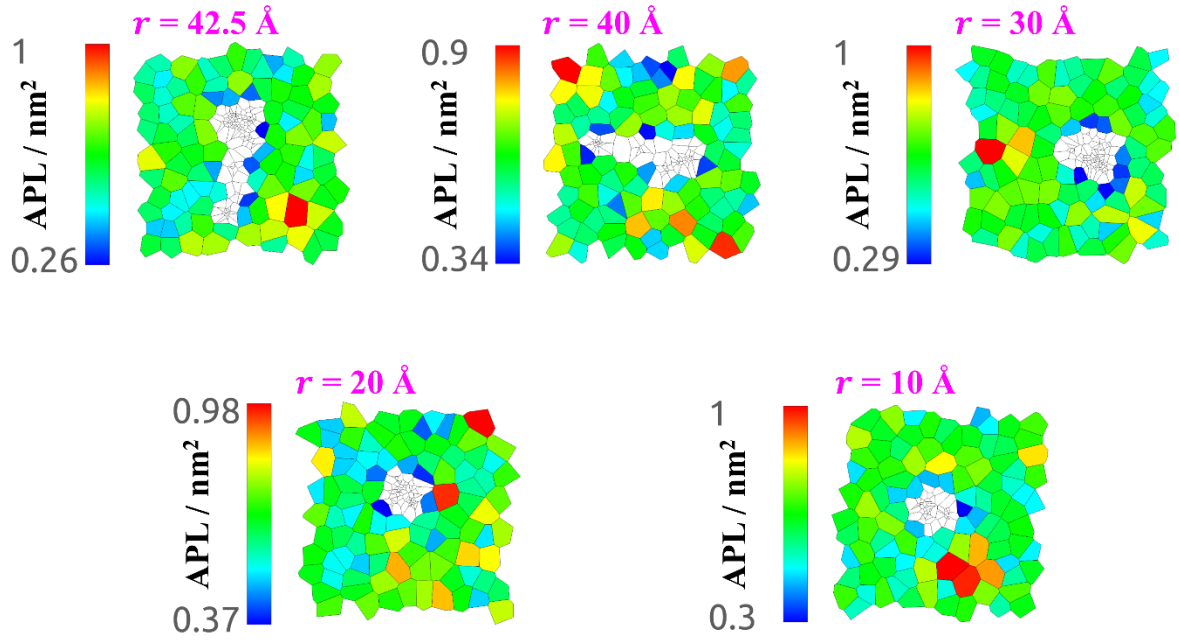

Figure 7: Voronoi cells associated with the area per lipid (APL) of lipids in the upper leaflet at r = 42.5, 40, 30, 20, and 10 Å. White areas in Voronoi diagrams correspond to the area occupied by pTB.

As seen in Fig. 6, both the APL and thickness of non-neighboring lipids, irrespective of r, remained close to the equilibrium value. The pTB is not present on the surface of the upper leaflet even at r = 45 Å and starts to touch the surface from the TS onwards. As a result, the APL of neighboring lipids from r = 42.5 Å onwards, decreases by ~ 35 % from the equilibrium value. The observed changes in the neighborhood of pTB during the insertion are because of the fact that the neighboring lipids need to make some spatial adjustments in order to occupy the inserted pTB channel. Interestingly, the APL even at the second lipid shell around pTB remained close to the equilibrium value, as seen in Fig. 7. The present result shows that the insertion of pTB causes only the local lateral compression of the membrane and proceeds as "nanoneedle" like one proposed in the penetration of the carbon nanotube into the membrane.[73] On the other hand, the thickness at neighboring lipids slightly increases by ~ 5 % from the equilibrium value. It has

been well-known that the gramicidin A channel has significant "hydrophobic mismatch," i.e., the difference between the lipid hydrophobic thickness and the peptide hydrophobic length.[74–77] In contrast, the hydrophobic mismatch is small for the pTB channel inside the POPC bilayer, leading to smaller bilayer distortions in thickness due to insertion.

CONCLUSIONS

The membrane insertion process of pTB is explored in detail using all-atom MD simulations. Our simulations show that the $\beta^{6.3}$-helix of pTB remained stable throughout the insertion process. The free energy calculations using the REUS simulations show that there is a small barrier of 4.3 kcal/mol located at the membrane surface for the membrane insertion of pTB from bulk water. Dissecting the free energy into enthalpic and entropic components reveals that the observed free energy barrier arises from the entropic bottleneck. Hence, it is considered that the free energy barrier for insertion becomes smaller when the temperature is lowered, which seems helpful for pTB to work well in low-temperature environments. Accordingly, it would be of interest to investigate the temperature dependence of the membrane insertion of pTB. The "shoulder" region in between the global free energy maximum and minimum corresponds to the trapping of pTB in the upper leaflet. The Voronoi cells associated with the APL suggest that the insertion of pTB proceeds with only the local lateral compression of the membrane. The small "hydrophobic mismatch" in the case of pTB helped the membrane thickness to remain almost constant during the insertion.

To elucidate the underlying mechanism of the vectorial membrane insertion of pTB, we performed multiple unbiased MD simulations. Our results reinforce the experimental observation of the spontaneous vectorial insertion of pTB into the membrane, led by the hydrophobic N-

terminal.[18] The spontaneous membrane insertion of pTB occurs in three consecutive phases: "landing," "penetration," and "equilibration" phases. Furthermore, our simulations reveal the presence of "trapped" and "untrapped" insertions, depending on whether or not pTB is trapped in the upper leaflet during the penetration phase, behind the free energy profile.

It has been known that molecular processes, such as chemical reactions, proceed in multiple pathways having fluctuating reaction rates at the single-molecule level, reflecting the existence of different local environments and a wide range of time scales for various fluctuations, i.e., static and dynamic disorders, in condensed phase systems including biomolecules.[78–81] The various trapped and untrapped trajectories found in the present study are manifestations of these disorders in the membrane insertion of pTB.

The present study is the first theoretical and computational study of the vectorial membrane insertion of a β-helical peptide, and provides useful insights to understand the vectorial insertion mechanism of other spontaneously inserting prefolded single transmembrane peptides. Our results on the vectorial insertion of pTB, where the membrane insertion of pTB from bulk water is anchored by the highly hydrophobic N-terminal blocking group (Mhe), further emphasize the significance of membrane anchoring for the vectorial insertion of transmembrane peptides. Since recently there have been several studies on the total synthesis[20,82,83] and the biomimetic synthesis[84,85] of pTB, understanding of the asymmetric structural features and vectorial membrane insertion of pTB can help in the de novo design of peptides and therapeutic drugs that can exhibit spontaneous vectorial insertion into target cell membranes.[86]

The cytotoxicity of pTB is related to its channel activity across the target cell membrane after spontaneously inserting into the membrane.[18] It has been reported in experiments that the pTB channel allows permeation of monovalent cations with the current in the order of $H^+ > Cs^+ > Rb^+ > K^+ > Na^+ > Li^+$.[18,21,22] Single-channel current recordings using planar lipid bilayer experiments in various ionic concentrations and membrane potentials reveal that the current-voltage curves are asymmetric with symmetric ionic concentrations across the membrane.[18,21,22] This phenomenon is called "rectification," i.e., the ionic flux from the C-terminal to the N-terminal is found to be higher than that from the opposite. In addition, experimental results suggest a "paradoxical" one-ion permeation mechanism such that ions permeate through the pTB channel by stepping between two binding sites in the pore, but never occupy these sites simultaneously.[21] For a better molecular understanding of these results, the ion-permeation through the pTB channel needs to be investigated in detail.

ASSOCIATED CONTENT

Supporting Information

The following files are available free of charge.

Components of the total potential energy using energy decomposition analysis, and the untrapped and trapped insertion trajectories which are not shown in the main text. (PDF)

Videos corresponding to the untrapped and trapped insertions shown in Figs. 4 and 5, respectively. (MPEG)

AUTHOR INFORMATION

ORCID IDs

Mahroof Kalathingal: 0000-0002-7126-9942

Takashi Sumikama: 0000-0003-3696-5720

Shigetoshi Oiki: 0000-0002-8438-6750

Shinji Saito: 0000-0003-4982-4820

Corresponding Author

*Email: oiki@u-fukui.ac.jp; Phone: +81-776-61-8695

*Email: shinji@ims.ac.jp; Phone: +81-564-55-7300

Notes

The authors declare no competing financial interest.

AUTHOR CONTRIBUTIONS

S.O. and S.S. designed research. M.K. performed research. M.K., T.S., and S.S. analyzed results. M.K. wrote the manuscript with suggestions from all authors.

ACKNOWLEDGMENTS

M.K. thanks the Ministry of Education, Culture, Sports, Science and Technology (MEXT) of the Government of Japan for financial support. This work is supported by JST, PRESTO, Japan (JPMJPR20K6) (T.S.), and Grant-in-Aid for Scientific Research (A) (JP20H00497) (S.O.) and (JP21H04676) (S.S.) from JSPS. The calculations are carried out at the Research Center for Computational Sciences in Okazaki.

REFERENCES

(1) Sandvig, K.; van Deurs, B. Membrane Traffic Exploited by Protein Toxins. *Annu. Rev. Cell Dev. Biol.* **2002**, *18* (1), 1–24.

(2) Minna M. Poranen; Rimantas Daugelavičius; Bamford, D. H. Common Principles in Viral Entry. *Annu. Rev. Microbiol.* **2002**, *56* (1), 521–538.

(3) Yeaman, M. R.; Yount, N. Y. Mechanisms of Antimicrobial Peptide Action and Resistance. *Pharmacol. Rev.* **2003**, *55* (1), 27–55.

(4) Bode, D. C.; Baker, M. D.; Viles, J. H. Ion Channel Formation by Amyloid-B42 Oligomers but Not Amyloid-B40 in Cellular Membranes. *J. Biol. Chem.* **2017**, *292* (4), 1404–1413.

(5) Zakharov, S. D.; Hulleman, J. D.; Dutseva, E. A.; Antonenko, Y. N.; Rochet, J.-C.; Cramer, W. A. Helical α-Synuclein Forms Highly Conductive Ion Channels. *Biochemistry* **2007**, *46* (50), 14369–14379.

(6) Georgieva, E. R.; Borbat, P. P.; Norman, H. D.; Freed, J. H. Mechanism of Influenza A M2 Transmembrane Domain Assembly in Lipid Membranes. *Sci. Rep.* **2015**, *5* (1), 11757.

(7) Leontiadou, H.; Mark, A. E.; Marrink, S. J. Antimicrobial Peptides in Action. *J. Am. Chem. Soc.* **2006**, *128* (37), 12156–12161.

(8) Mihajlovic, M.; Lazaridis, T. Antimicrobial Peptides in Toroidal and Cylindrical Pores. *Biochim. Biophys. Acta - Biomembr.* **2010**, *1798* (8), 1485–1493.

(9) Sengupta, D.; Leontiadou, H.; Mark, A. E.; Marrink, S.-J. Toroidal Pores Formed by Antimicrobial Peptides Show Significant Disorder. *Biochim. Biophys. Acta - Biomembr.* **2008**, *1778* (10), 2308–2317.

(10) Ulmschneider, M. B.; Doux, J. P. F.; Killian, J. A.; Smith, J. C.; Ulmschneider, J. P. Mechanism and Kinetics of Peptide Partitioning into Membranes from All-Atom Simulations of Thermostable Peptides. *J. Am. Chem. Soc.* **2010**, *132* (10), 3452–3460.

(11) Ulmschneider, M. B.; Smith, J. C.; Ulmschneider, J. P. Peptide Partitioning Properties from Direct Insertion Studies. *Biophys. J.* **2010**, *98* (12), L60–L62.

(12) Ulmschneider, J. P.; Smith, J. C.; White, S. H.; Ulmschneider, M. B. In Silico Partitioning and Transmembrane Insertion of Hydrophobic Peptides under Equilibrium Conditions. *J. Am. Chem. Soc.* **2011**, *133* (39), 15487–15495.

(13) Ulmschneider, M. B.; Ulmschneider, J. P.; Schiller, N.; Wallace, B. A.; von Heijne, G.; White, S. H. Spontaneous Transmembrane Helix Insertion Thermodynamically Mimics Translocon-Guided Insertion. *Nat. Commun.* **2014**, *5* (1), 4863.

(14) Hamada, T.; Sugawara, T.; Matsunaga, S.; Fusetani, N. Polytheonamides, Unprecedented Highly Cytotoxic Polypeptides, from the Marine Sponge Theonella Swinhoei. *Tetrahedron Lett.* **1994**, *35* (5), 719–720.

(15) Oiki, S.; Muramatsu, I.; Matsunaga, S.; Fusetani, N. A Channel-Forming Peptide Toxin: Polytheonamide from Marine Sponge (Theonella Swinhoei). *Nihon Yakurigaku Zasshi.* **1997**, *110* (Suppl. 1), 195P-198P.

(16) Hamada, T.; Matsunaga, S.; Yano, G.; Fusetani, N. Polytheonamides A and B, Highly Cytotoxic, Linear Polypeptides with Unprecedented Structural Features, from the Marine Sponge, Theonella Swinhoei. *J. Am. Chem. Soc.* **2005**, *127* (1), 110–118.

(17) Hamada, T.; Matsunaga, S.; Fujiwara, M.; Fujita, K.; Hirota, H.; Schmucki, R.; Güntert, P.; Fusetani, N. Solution Structure of Polytheonamide B, a Highly Cytotoxic Nonribosomal Polypeptide from Marine Sponge. *J. Am. Chem. Soc.* **2010**, *132* (37), 12941–12945.

(18) Iwamoto, M.; Shimizu, H.; Muramatsu, I.; Oiki, S. A Cytotoxic Peptide from a Marine Sponge Exhibits Ion Channel Activity through Vectorial-Insertion into the Membrane. *FEBS Lett.* **2010**, *584* (18), 3995–3999.

(19) Mori, T.; Kokubo, H.; Oiki, S.; Okamoto, Y. Dynamic Structure of the Polytheonamide B Channel Studied by Normal Mode Analysis. *Mol. Simul.* **2011**, *37* (12), 975–985.

(20) Shinohara, N.; Itoh, H.; Matsuoka, S.; Inoue, M. Selective Modification of the N-Terminal Structure of Polytheonamide B Significantly Changes Its Cytotoxicity and Activity as an Ion Channel. *ChemMedChem* **2012**, *7* (10), 1770–1773.

(21) Iwamoto, M.; Matsunaga, S.; Oiki, S. Paradoxical One-Ion Pore Behavior of the Long β-Helical Peptide of Marine Cytotoxic Polytheonamide B. *Sci. Rep.* **2014**, *4*, 3636.

(22) Matsuki, Y.; Iwamoto, M.; Mita, K.; Shigemi, K.; Matsunaga, S.; Oiki, S. Rectified Proton Grotthuss Conduction Across a Long Water-Wire in the Test Nanotube of the Polytheonamide B Channel. *J. Am. Chem. Soc.* **2016**, *138* (12), 4168–4177.

(23) Kalathingal, M.; Sumikama, T.; Mori, T.; Oiki, S.; Saito, S. Structure and Dynamics of Solvent Molecules inside the Polytheonamide B Channel in Different Environments: A Molecular Dynamics Study. *Phys. Chem. Chem. Phys.* **2018**, *20* (5), 3334–3348.

(24) Andersen, O. S.; Koeppe, R. E.; Roux, B. Gramicidin Channels. *IEEE Trans. Nanobioscience* **2005**, *4* (1), 10–20.

(25) Renevey, A.; Riniker, S. The Importance of N-Methylations for the Stability of the B6.3 -Helical Conformation of Polytheonamide B. *Eur. Biophys. J.* **2017**, *46* (4), 363–374.

(26) Iwamoto, M.; Oiki, S. Contact Bubble Bilayers with Flush Drainage. *Sci. Rep.* **2015**, *5*, 9110.

(27) Iwamoto, M.; Oiki, S. Membrane Perfusion of Hydrophobic Substances Around Channels Embedded in the Contact Bubble Bilayer. *Sci. Rep.* **2017**, *7* (1), 6857.

(28) Johansson, A. C. V.; Lindahl, E. Position-Resolved Free Energy of Solvation for Amino Acids in Lipid Membranes from Molecular Dynamics Simulations. *Proteins Struct. Funct. Bioinforma.* **2007**, *70* (4), 1332–1344.

(29) MacCallum, J. L.; Bennett, W. F. D.; Tieleman, D. P. Partitioning of Amino Acid Side Chains into Lipid Bilayers: Results from Computer Simulations and Comparison to Experiment. *J. Gen. Physiol.* **2007**, *129* (5), 371–377.

(30) Dorairaj, S.; Allen, T. W. On the Thermodynamic Stability of a Charged Arginine Side Chain in a Transmembrane Helix. *Proc. Natl. Acad. Sci.* **2007**, *104* (12), 4943–4948.

(31) Gumbart, J.; Chipot, C.; Schulten, K. Free-Energy Cost for Translocon-Assisted Insertion of Membrane Proteins. *Proc. Natl. Acad. Sci.* **2011**, *108* (9), 3596–3601.

(32) Gumbart, J.; Roux, B. Determination of Membrane-Insertion Free Energies by Molecular Dynamics Simulations. *Biophys. J.* **2012**, *102* (4), 795–801.

(33) Gumbart, J. C.; Ulmschneider, M. B.; Hazel, A.; White, S. H.; Ulmschneider, J. P. Computed Free Energies of Peptide Insertion into Bilayers Are Independent of Computational Method. *J. Membr. Biol.* **2018**, *251* (3), 345–356.

(34) Babakhani, A.; Gorfe, A. A.; Kim, J. E.; McCammon, J. A. Thermodynamics of Peptide Insertion and Aggregation in a Lipid Bilayer. *J. Phys. Chem. B* **2008**, *112* (34), 10528–10534.

(35) Irudayam, S. J.; Pobandt, T.; Berkowitz, M. L. Free Energy Barrier for Melittin Reorientation from a Membrane-Bound State to a Transmembrane State. *J. Phys. Chem. B* **2013**, *117* (43), 13457–13463.

(36) Yeh, I.-C.; Olson, M. A.; Lee, M. S.; Wallqvist, A. Free-Energy Profiles of Membrane Insertion of the M2 Transmembrane Peptide from Influenza A Virus. *Biophys. J.* **2008**, *95* (11), 5021–5029.

(37) Tieleman, D. P.; Sansom, M. S. P. Molecular Dynamics Simulations of Antimicrobial Peptides: From Membrane Binding to Trans-Membrane Channels. *Int. J. Quantum Chem.* **2001**, *83* (3–4), 166–179.

(38) Santo, K. P.; Berkowitz, M. L. Difference between Magainin-2 and Melittin Assemblies in Phosphatidylcholine Bilayers: Results from Coarse-Grained Simulations. *J. Phys. Chem. B* **2012**, *116* (9), 3021–3030.

(39) Santo, K. P.; Irudayam, S. J.; Berkowitz, M. L. Melittin Creates Transient Pores in a Lipid Bilayer: Results from Computer Simulations. *J. Phys. Chem. B* **2013**, *117* (17), 5031–5042.

(40) Pokhrel, R.; Bhattarai, N.; Baral, P.; Gerstman, B. S.; Park, J. H.; Handfield, M.; Chapagain, P. P. Molecular Mechanisms of Pore Formation and Membrane Disruption by the Antimicrobial Lantibiotic Peptide Mutacin 1140. *Phys. Chem. Chem. Phys.* **2019**, *21* (23), 12530–12539.

(41) Deng, Y.; Qian, Z.; Luo, Y.; Zhang, Y.; Mu, Y.; Wei, G. Membrane Binding and Insertion of a PHLIP Peptide Studied by All-Atom Molecular Dynamics Simulations. *Int. J. Mol. Sci.* **2013**, *14* (7), 14532–14549.

(42) Yue, T.; Sun, M.; Zhang, S.; Ren, H.; Ge, B.; Huang, F. How Transmembrane Peptides Insert and Orientate in Biomembranes: A Combined Experimental and Simulation Study. *Phys. Chem. Chem. Phys.* **2016**, *18* (26), 17483–17494.

(43) Herce, H. D.; Garcia, A. E. Molecular Dynamics Simulations Suggest a Mechanism for Translocation of the HIV-1 TAT Peptide across Lipid Membranes. *Proc. Natl. Acad. Sci.* **2007**, *104* (52), 20805–20810.

(44) Nymeyer, H.; Woolf, T. B.; Garcia, A. E. Folding Is Not Required for Bilayer Insertion: Replica Exchange Simulations of an α-Helical Peptide with an Explicit Lipid Bilayer. *Proteins Struct. Funct. Bioinforma.* **2005**, *59* (4), 783–790.

(45) Im, W.; Brooks, C. L. Interfacial Folding and Membrane Insertion of Designed Peptides Studied by Molecular Dynamics Simulations. *Proc. Natl. Acad. Sci.* **2005**, *102* (19), 6771–6776.

(46) Ulmschneider, M. B.; Ulmschneider, J. P. Folding Peptides into Lipid Bilayer Membranes. *J. Chem. Theory Comput.* **2008**, *4* (11), 1807–1809.

(47) Ulmschneider, J. P.; Doux, J. P. F.; Killian, J. A.; Smith, J. C.; Ulmschneider, M. B. Peptide Partitioning and Folding into Lipid Bilayers. *J. Chem. Theory Comput.* **2009**, *5* (9), 2202–2205.

(48) Maier, J. A.; Martinez, C.; Kasavajhala, K.; Wickstrom, L.; Hauser, K. E.; Simmerling, C. Ff14SB: Improving the Accuracy of Protein Side Chain and Backbone Parameters from Ff99SB. *J. Chem. Theory Comput.* **2015**, *11* (8), 3696–3713.

(49) Jorgensen, W. L.; Chandrasekhar, J.; Madura, J. D.; Impey, R. W.; Klein, M. L. Comparison of Simple Potential Functions for Simulating Liquid Water. *J. Chem. Phys.* **1983**, *79* (2), 926–935.

(50) Dickson, C. J.; Madej, B. D.; Skjevik, Å. A.; Betz, R. M.; Teigen, K.; Gould, I. R.; Walker, R. C. Lipid14: The Amber Lipid Force Field. *J. Chem. Theory Comput.* **2014**, *10* (2), 865–879.

(51) Joung, I. S.; Cheatham, T. E. Determination of Alkali and Halide Monovalent Ion Parameters for Use in Explicitly Solvated Biomolecular Simulations. *J. Phys. Chem. B* **2008**, *112* (30), 9020–9041.

(52) Case, D. A.; Ben-Shalom, I. Y.; Brozell, S. R.; Cerutti, D. S.; Cheatham, T. E.; III; Cruzeiro, V. W. D.; Darden, T. A.; Duke, R. E.; Ghoreishi, D.; Gilson, M. K.; Gohlke, H.; Goetz, A. W.; Greene, D.; Harris, R.; Homeyer, N.; Huang, Y.; Izadi, S.; Kovalenko, A.; Kurtzman, T.; Lee, T. S.; LeGrand, S.; Li, P.; Lin, C.; Liu, J.; Luchko, T.; Luo, R.; Mermelstein, D. J.; Merz, K. M.; Miao, Y.; Monard, G.; Nguyen, C.; Nguyen, H.; Omelyan, I.; Onufriev, A.; Pan, F.; Qi, R.; Roe, D. R.; Roitberg, A.; Sagui, C.; Schott-Verdugo, S.; Shen, J.; Simmerling, C. L.; Smith, J.; Salomon-Ferrer, R.; Swails, J.; Walker, R. C.; Wang, J.; Wei, H.; Wolf, R. M.; Wu, X.; Xiao, L.; York, D. M.; Kollman, P. A. AMBER 2018, University of California, San Francisco. 2018.

(53) Ryckaert, J.-P.; Ciccotti, G.; Berendsen, H. J. C. Numerical Integration of the Cartesian Equations of Motion of a System with Constraints: Molecular Dynamics of n-Alkanes. *J. Comput. Phys.* **1977**, *23* (3), 327–341.

(54) Darden, T.; York, D.; Pedersen, L. Particle Mesh Ewald: An $N \cdot \log(N)$ Method for Ewald Sums in Large Systems. *J. Chem. Phys.* **1993**, *98* (12), 10089–10092.

(55) Pastor, R. W.; Brooks, B. R.; Szabo, A. An Analysis of the Accuracy of Langevin and Molecular Dynamics Algorithms. *Mol. Phys.* **1988**, *65* (6), 1409–1419.

(56) Berendsen, H. J. C.; Postma, J. P. M.; van Gunsteren, W. F.; DiNola, A.; Haak, J. R. Molecular Dynamics with Coupling to an External Bath. *J. Chem. Phys.* **1984**, *81* (8), 3684–3690.

(57) Jo, S.; Lim, J. B.; Klauda, J. B.; Im, W. CHARMM-GUI Membrane Builder for Mixed Bilayers and Its Application to Yeast Membranes. *Biophys. J.* **2009**, *97* (1), 50–58.

(58) Press, W. H.; Teukolsky, S. A.; Vetterling, W. T.; Flannery, B. P. *Numerical Recipes 3rd Edition: The Art of Scientific Computing*; Cambridge University Press, 2007.

(59) Kučerka, N.; Nieh, M.-P.; Katsaras, J. Fluid Phase Lipid Areas and Bilayer Thicknesses of Commonly Used Phosphatidylcholines as a Function of Temperature. *Biochim. Biophys. Acta - Biomembr.* **2011**, *1808* (11), 2761–2771.

(60) Torrie, G. M.; Valleau, J. P. Nonphysical Sampling Distributions in Monte Carlo Free-Energy Estimation: Umbrella Sampling. *J. Comput. Phys.* **1977**, *23* (2), 187–199.

(61) Park, S.; Kim, T.; Im, W. Transmembrane Helix Assembly by Window Exchange Umbrella Sampling. *Phys. Rev. Lett.* **2012**, *108* (10), 108102.

(62) Kumar, S.; Rosenberg, J. M.; Bouzida, D.; Swendsen, R. H.; Kollman, P. A. THE Weighted Histogram Analysis Method for Free-energy Calculations on Biomolecules. I. The Method. *J. Comput. Chem.* **1992**, *13* (8), 1011–1021.

(63) Kumar, S.; Rosenberg, J. M.; Bouzida, D.; Swendsen, R. H.; Kollman, P. A. Multidimensional Free-energy Calculations Using the Weighted Histogram Analysis Method. *J. Comput. Chem.* **1995**, *16* (11), 1339–1350.

(64) Grossfield, A. WHAM: The Weighted Histogram Analysis Method, Version 2.0.10.

(65) Roe, D. R.; Cheatham, T. E. PTRAJ and CPPTRAJ: Software for Processing and Analysis of Molecular Dynamics Trajectory Data. *J. Chem. Theory Comput.* **2013**, *9* (7), 3084–3095.

(66) Lukat, G.; Krüger, J.; Sommer, B. APL@Voro: A Voronoi-Based Membrane Analysis Tool for GROMACS Trajectories. *J. Chem. Inf. Model.* **2013**, *53* (11), 2908–2925.

(67) Humphrey, W.; Dalke, A.; Schulten, K. VMD - Visual Molecular Dynamics. *J. Mol. Graph.* **1996**, *14*, 33–38.

(68) Doktorova, M.; LeVine, M. V.; Khelashvili, G.; Weinstein, H. A New Computational Method for Membrane Compressibility: Bilayer Mechanical Thickness Revisited. *Biophys. J.* **2019**, *116* (3), 487–502.

(69) Feller, S. E.; Pastor, R. W. Constant Surface Tension Simulations of Lipid Bilayers: The Sensitivity of Surface Areas and Compressibilities. *J. Chem. Phys.* **1999**, *111* (3), 1281–1287.

(70) Kraszewski, S.; Bianco, A.; Tarek, M.; Ramseyer, C. Insertion of Short Amino-Functionalized Single-Walled Carbon Nanotubes into Phospholipid Bilayer Occurs by Passive Diffusion. *PLoS One* **2012**, *7* (7), e40703.

(71) Mitchell-Koch, K. R.; Thompson, W. H. How Important Is Entropy in Determining the Position-Dependent Free Energy of a Solute in a Nanoconfined Solvent? *J. Phys. Chem. C* **2007**, *111* (32), 11991–12001.

(72) Sun, D.; He, S.; Bennett, W. F. D.; Bilodeau, C. L.; Andersen, O. S.; Lightstone, F. C.; Ingólfsson, H. I. Atomistic Characterization of Gramicidin Channel Formation. *J. Chem. Theory Comput.* **2021**, *17* (1), 7–12.

(73) Kostarelos, K.; Lacerda, L.; Pastorin, G.; Wu, W.; Wieckowski, S.; Luangsivilay, J.; Godefroy, S.; Pantarotto, D.; Briand, J.-P.; Muller, S.; Prato, M.; Bianco, A. Cellular Uptake of Functionalized Carbon Nanotubes Is Independent of Functional Group and Cell Type. *Nat. Nanotechnol.* **2007**, *2*, 108.

(74) Yoo, J.; Cui, Q. Membrane-Mediated Protein-Protein Interactions and Connection to Elastic Models: A Coarse-Grained Simulation Analysis of Gramicidin A Association. *Biophys. J.* **2013**, *104* (1), 128–138.

(75) Nielsen, C.; Andersen, O. S. Inclusion-Induced Bilayer Deformations: Effects of Monolayer Equilibrium Curvature. *Biophys. J.* **2000**, *79* (5), 2583–2604.

(76) Bruno, M. J.; Koeppe, R. E.; Andersen, O. S. Docosahexaenoic Acid Alters Bilayer Elastic Properties. *Proc. Natl. Acad. Sci.* **2007**, *104* (23), 9638–9643.

(77) Sodt, A. J.; Beaven, A. H.; Andersen, O. S.; Im, W.; Pastor, R. W. Gramicidin A Channel Formation Induces Local Lipid Redistribution II: A 3D Continuum Elastic Model. *Biophys. J.* **2017**, *112* (6), 1198–1213.

(78) Zwanzig, R. Rate Processes with Dynamical Disorder. *Acc. Chem. Res.* **1990**, *23* (5), 148–152.

(79) Lu, H. P. Single-Molecule Enzymatic Dynamics. *Science (80-.).* **1998**, *282* (5395), 1877–1882.

(80) Moerner, W. E. Illuminating Single Molecules in Condensed Matter. *Science (80-.).* **1999**, *283* (5408), 1670–1676.

(81) Weiss, S. Fluorescence Spectroscopy of Single Biomolecules. *Science (80-.).* **1999**, *283* (5408), 1676–1683.

(82) Inoue, M.; Shinohara, N.; Tanabe, S.; Takahashi, T.; Okura, K.; Itoh, H.; Mizoguchi, Y.; Iida, M.; Lee, N.; Matsuoka, S. Total Synthesis of the Large Non-Ribosomal Peptide Polytheonamide B. *Nat Chem* **2010**, *2* (4), 280–285.

(83) Itoh, H.; Inoue, M. Chemical Construction and Structural Permutation of Potent Cytotoxin Polytheonamide B: Discovery of Artificial Peptides with Distinct Functions. *Acc. Chem. Res.* **2013**, *46* (7), 1567–1578.

(84) Freeman, M. F.; Gurgui, C.; Helf, M. J.; Morinaka, B. I.; Uria, A. R.; Oldham, N. J.; Sahl, H.-G.; Matsunaga, S.; Piel, J. Metagenome Mining Reveals Polytheonamides as Posttranslationally Modified Ribosomal Peptides. *Science (80-.).* **2012**.

(85) Freeman, M. F.; Helf, M. J.; Bhushan, A.; Morinaka, B. I.; Piel, J. Seven Enzymes Create Extraordinary Molecular Complexity in an Uncultivated Bacterium. *Nat. Chem.* **2017**, *9* (4), 387–395.

(86) Wimley, W. C.; White, S. H. Designing Transmembrane α-Helices That Insert Spontaneously †. *Biochemistry* **2000**, *39* (15), 4432–4442.